Supporting Information

Molecular Scissoring Strategy to Modify Band Gap and Molecular Motion for High-Performance Solar Desalination and Water Purification

Zishuo Zhang [1], Fangqing Fan [1], Jingshuai Zhu [2] *, Minyi Liang [3], Hongyu He [4], Youxun, Wang [1], Xuemei Chen [1], Ning Weng [1], Shuyan Mai [1], Jiaxin Zheng [5], Shiguo Chen [1] *, and Yuanfeng Wang [1] *

[1] College of Materials Science and Engineering, Shenzhen University, Shenzhen, 518060, China

[2] School of Fashion and Textiles, The Hong Kong Polytechnic University, Kowloon, 999077, Hong Kong

[3] Ningbo Customs Technology Center, Ningbo, 315192, China

[4] Ningbo Joysun Product Testing Service Compan, Ningbo, 315012, China

[5] School of Advanced Materials, Peking University Shenzhen Graduate School, Shenzhen, 518055, China

* Corresponding Author E-mail: jingshuai.zhu@polyu.edu.hk, csg@szu.edu.cn, wangyuanfeng@szu.edu.cn

Experimental Section

Chemicals and Materials

Unless otherwise stated, all the chemical reagents used in the research process are procured and can be used directly without further purification. Among them, the synthesis of IEIC-4F and ITIC-4F was carried out according to method reported previously[1, 2] Various types of wood sponges used as the base of the evaporator can be procured commercially. The quartz crucibles used for testing the photothermal conversion efficiency, as well as the 808 nm lasers with powers of 1.0 W cm^{-2} and 0.8 W cm^{-2}, are all purchased from commercial platform. The chloroform reagent is produced by Shenzhen Bolaien Technology Co., Ltd. The simulated seawater is prepared in the laboratory, and the formula is as follows: NaCl: 27100 mg L^{-1}, $MgCl_2$: 5000 mg L^{-1}, $CaCl_2$: 1300 mg L^{-1}, KCl: 800 mg L^{-1}.

Synthesis

IEIC-4F

Compound 1 (115 mg, 0.5 mmol), compound 2 (108 mg, 0.1 mmol), pyridine (0.6 ml), and chloroform (20 ml) were added to a three-necked round-bottom flask. The mixture was then deoxygenated with nitrogen for 20 min and stirred for 15 h. After cooling to room temperature, the mixture was poured into methanol (100 ml) and filtered. The residue was purified by silica gel column chromatography using petroleum ether: chloroform (1:1.5) as the eluent, yielding a dark green solid (110 mg, 73%). ^{1}H NMR (600 MHz, $CDCl_3$): δ 8.76 (s, 2H), 8.54 (dd, J = 9.9, 6.4 Hz, 2H), 7.67 (t, J = 7.5 Hz, 2H), 7.61 (s, 2H), 7.48 (d, J = 20.9 Hz, 4H), 7.19 (d, J = 8.1 Hz, 8H), 7.11 (d, J = 8.2 Hz, 8H), 2.79 (d, J = 7.3 Hz, 4H), 2.59 (t, J = 7.8 Hz, 8H), 1.75 (t, 2H), 1.64 – 1.57 (m, 8H), 1.41 – 1.20 (m, 40H), 0.94 – 0.80 (m, 24H), ^{13}C NMR (100 MHz, $CDCl_3$): δ

186.22, 158.43, 157.71, 155.51, 154.51, 153.75, 151.37, 149.75, 145.69, 142.15, 141.10, 140.36, 138.02, 137.64, 136.80, 135.72, 134.61, 134.04, 128.73, 127.98, 124.76, 121.37, 118.20, 115.19, 114.44, 112.79, 69.81, 63.30, 39.49, 35.76, 33.94, 32.56, 31.88, 31.51, 29.28, 28.72, 25.80, 23.18, 22.78, 14.24, 10.71. MS (MALDI-TOF): *m/z* 1499.18 (M^+).

ITIC-4F

Compound 3 (115 mg, 0.5 mmol), compound 4 (135 mg, 0.1 mmol), pyridine (0.6 ml), and chloroform (20 ml) were added to a three-necked round-bottom flask. The mixture was then deoxygenated with nitrogen for 20 min and stirred for 15 h. After cooling to room temperature, the mixture was poured into methanol (100 ml) and filtered. The residue was purified by silica gel column chromatography using petroleum ether: chloroform (1:1.5) as the eluent, yielding a black solid (123 mg, 69%). ^{1}H NMR (600 MHz, $CDCl_3$): δ 8.79 (s, 2H), 8.46 (dd, J = 9.8, 6.4 Hz, 2H), 8.19 (s, 2H), 7.66 – 7.59 (m, 4H), 7.16 (d, J = 8.4 Hz, 8H), 7.09 (d, J = 8.4 Hz, 8H), 2.54 – 2.47 (m, 8H), 1.57 – 1.48 (m, 8H), 1.28 – 1.21 (m, 24H), 0.82 – 0.78 (m, 12H), ^{13}C NMR (151 MHz, $CDCl_3$) δ 185.87, 158.40, 155.86, 155.33, 153.75, 147.75, 143.99, 142.62, 139.47, 138.81, 138.55, 137.71, 137.07, 136.61, 134.50, 128.91, 121.72, 118.72, 115.05, 114.25, 112.81, 69.73, 63.26, 58.01, 35.61, 31.71, 31.29, 29.18, 22.60, 18.19, 14.07. MS (MALDI-TOF): *m/z* 1775.04 (M^+).

Characterization

Molecular structures were characterized by MALDI-TOF/TOF mass spectrometry (Bruker autoflex speed) and ^{13}C/^{1}H NMR spectroscopy (Bruker AVANCE III). UV-Vis-NIR absorption spectra of spin-coated thin-film samples and solution samples (1 mg/100 mL in $CHCl_3$) were recorded using a UV-Vis-NIR spectrophotometer

(Shimadzu UV-3600i Plus). UPS spectra were acquired by an X-ray photoelectron spectrometer (ESCALAB 250xi). Contact angles were determined using a contact angle analyzer (Contact Angle System OCA 25). Evaporator performance evaluation: Simulated sunlight was generated by a xenon lamp solar simulator (CMS-SL500). Water evaporation rates and efficiency were calculated through mass variation measurements with an electronic balance (BL-C). At the same time, environmental temperature and humidity were monitored using a thermohygrometer (Delixi THM-01). Light power calibration was performed with a solar power meter (TES 132). During the experiments, the model of the laser used is HEX808800D-AL and HEX8081000D-AL and the surface temperature was recorded by an infrared camera (FLIR E95 24°). Thermogravimetric analysis (TGA) and differential scanning calorimetry (DSC) were performed on a simultaneous thermal analyzer (Netzsch STA 409PC). SEM images were obtained using a field emission scanning electron microscope (TESCAN MIRA LMS). CLSM images is captured using an Olympus microscope.

Molecular simulations

Density functional theory (DFT) calculations were performed using the Gaussian 09 software.[3] The B3LYP functional, integrated with the D3BJ dispersion correction,[4] was applied throughout the computations. For geometry optimization and frequency analysis of molecules, the 6-311G(d) basis set was employed.[5] Subsequently, the Multiwfn[6] and VMD[7] software were utilized to extract and visualize molecular orbitals.

Molecular Dynamics Simulation

Atomistic molecular dynamics simulations have been performed in the

GROMACS[8] (version 2022.6) simulation package, using the General Amber force field (GAFF2). 100 chains of IEIC-4F and ITIC-4F were randomly inserted into separate cubic boxes of around 11 nm. After thousands of steps of energy minimization, the systems were equilibrated under the NPT ensemble for 20 ns at relatively high temperature of 600 K to fully randomize the molecules and followed the production runs for another 20 ns. The final temperature was coupled to 298 K using the Nose-Hoover method and the pressure was coupled to 1 atm using the Parrinello-Rahman method. The cutoff scheme of 1.2 nm was implemented for the non-bonded interactions, and the Particle Mesh Ewald method[9] with a fourierspacing of 0.1 nm was applied for the long range electrostatic interactions. All covalent bonds with hydrogen atoms were constraint using the LINCS algorithm.[10]

The calculation of molar extinction coefficient

The molar extinction coefficient (ε) was calculated using the Beer-Lambert Law:

$A = \varepsilon c L$

Where: A is the absorbance (measured via UV-Vis spectroscopy),

c is molar concentration (m L^{-1}),

L is path length (1 cm quartz cuvette).

	ITIC-4F	IEIC-4F
The absorbance of the absorption peak	0.4544	0.5173
absorption peak position (nm)	691	715
molar concentration (m^{-1} L^{-1})	6.67×10^{-6}	5.56×10^{-6}
ε (m^{-1} cm^{-1})	6.81×10^{4}	9.29×10^{4}

Calculation of the photothermal conversion efficiency

Method: Laser irradiation was conducted with a laser system, and temperature data was captured by an infrared camera (FLIR E95 24°). Heat capacity was determined via the sapphire method using a differential scanning calorimeter (Mettler DSC3).

Certain calculations in the procedures were adapted from prior approaches.[11, 12] Details are as follows:

Based on the total energy balance for this system:

$$Q_S = Q_{heat} + Q_{loss}$$

Where Q_S is the photothermal heat energy inputted by irradiating NIR laser to powder samples, Q_{heat} is thermal energy that required to raise the temperature of the powder, and Q_{loss} is thermal energy dissipated to the ambient surroundings. (air and quartz crucible)

$$Q_{heat} = m\bar{C}_p\Delta T_{max}$$

Where m is the mass of the sample powder used in the experiment, $\bar{C}_p$ is the average specific heat capacity of the sample during the temperature increase, and ΔT is the temperature rise of the sample.

$$Q_{loss} = hS\Delta T_{max}$$

Where h is heat transfer coefficient, S is the surface area of the container, ΔT_{max} is the temperature rise of the sample.

In order to obtain the hS, a dimensionless driving force temperature, θ is introduced as follows:

$$\theta = \frac{T - T_{surr}}{T_{max} - T_{surr}}$$

When the temperature is maximum, the system is in balance:

$$Q_S = Q_{loss} = hS\Delta T_{max}$$

Where T is the temperature of powder, T_{max} is the maximum system temperature, and T_{surr} is the initial temperature.

The sample system time constant τ_S

$$\tau_S = \frac{m\bar{C}_p}{hS}$$

thus: $\frac{d\theta}{dt} = \frac{1}{\tau_s hS\Delta T_{max}} Q_s - \frac{\theta}{\tau_S}$

When the laser is off, $Q_S = 0$, therefore: $\frac{d\theta}{dt} = -\frac{\theta}{\tau_S}$ and $t = -\tau_s \ln\theta$

Therefore, hS could be calculated from the slope of cooling time vs $\ln\theta$.

$$Q_{in} = I\left(1 - 10^{-A_{808}}\right) \times \Delta t$$

Where I is the laser power (0.8 W cm^{-2}), A808 is the absorbance of the samples at the wavelength of 808 nm. and Δt is the time required for the sample to rise to the maximum temperature.

$$\eta = \frac{Q_s}{Q_{in}}$$

Using the values in the following table and the previously derived equations, the photothermal conversion efficiencies for IEIC-4F and ITIC-4F were determined. (**Figure S9-11**)

	IEIC-4F	ITIC-4F
m (mg)	11.22	11.49
$\bar{C}_p$ (J T^{-1} g^{-1})	2.504	1.482
T_{surr} (°C)	26.0	30.5
T_{max} (°C)	252.2	262.1

ΔT_{max} (°C)	226.2	231.6
τ_S	7.88	6.74
ΔT_{max} (J T^{-1})	0.003565	0.002526
A_{808}	0.713	0.376
Δt (s)	20.0	17.9
Q_{heat} (J)	6.349	3.944
Q_{loss} (J)	0.805	0.585
Q_S (J)	7.154	4.529
Q_{in} (J)	12.900 13.4	8.295 11.7
η	55.5%	54.6%

Characterization of the thermal conductivity of two types of sponge substrates

Using the Hot Disk method/transient plane source method and a thermal conductivity meter, and in accordance with the standard of ISO22007-2, the thermal conductivities of two types of sponges with different micro-nano structures are measured in an environment at 65 °C.

The measured thermal conductivity of the sponge with a hierarchical porous structure is 0.07750 W mK^{-1}, and the thermal conductivity of the material with only macroporous diameters is 0.2514 W mK^{-1}.

Numerical simulation

This calculation employs the finite element calculation method. By leveraging the geometric optics module and the solid and liquid heat transfer modules of the COMSOL Multiphysics software, a coupling is performed to simulate the temperature field distribution of two types of sponge materials with different pore sizes when they are illuminated. At the initial stage of the simulation, three-dimensional geometric models of two types of sponge materials (with only large pores, and with hierarchical pores) were established. The internal random pores of these models were generated by inserting code, and the porosities of the two structures were kept consistent. The sponge materials were immersed in water, and a light source was set at the top to radiatively heat the system.

The geometric optics module, as well as the solid and liquid heat transfer modules, were added. Subsequently, the thermal properties of the materials in the model were set, including thermal conductivity, specific heat capacity, and density. All the material parameters were set as required in the following table. The light source simulated conical bundle rays, which were absorbed and generated heat after irradiating the sponge materials (the heat was calculated through built-in functions). The power of the light source was showed in the following table, but it was slightly adjusted during the simulation debugging process to closely match the experimental results as much as possible. Since the pore size of the small pores was relatively small, a finer mesh was used during the meshing process. The ray tracing program was adopted for the light path and absorption; the temperature field simulation used a transient calculation program, enabling the acquisition of the temperature distribution at any time point.

	Hierarchical porous structure	Only macroporous structure

Thermal conductivity of the material	0.07750 W mK^{-1}	0.2514 W mK^{-1}
Density of lignin material	7500 kg m^{-3}	
Constant-pressure heat capacity (C_p) of lignin material	1350 J kg^{-1} K^{-1}	
Bulk dimensions (Radius × Height)	3.14 × (1 × 1) cm^2 × 1 cm	
Power density of light source	1000W m^{-2}	

Method of Manufacturing the Evaporator

Dissolve IEIC-4F and ITIC-4F in chloroform solution at a concentration of 1 mg per 100 μL. Since both IEIC-4F and ITIC-4F have excellent solubility in chloroform, no other treatment is required. Use a pipette to suck up the solution, and then load it onto the sponge substrate at a dosage of 100 μL per 1 cm^2. Place it in a fume hood to air-dry (1 h). Once all the chloroform has evaporated, the preparation is completed.

Solar steam generation experiments

Place a circular evaporator with a diameter of 1 cm in a small beaker. Under the illumination of a xenon lamp light source with an intensity of 1 sun, use the timing shooting function of a digital camera to take pictures and record the readings of the

electronic balance every 5 minutes. Record the mass change of the electronic balance within 120 minutes. Perform linear fitting on the measured data points, select the evaporation curve within 60 minutes among them and calculate the evaporation rate.

Calculation of the efficiency for solar to vapor generation[13]

The conversion efficiency η of solar energy in photothermally assisted water evaporation was calculated using the following formula:

$$\eta = \dot{m} h_{LV} / qi$$

Where $\dot{m}$ denotes the solar water evaporation rate of water under solar illumination ($\dot{m} = \dot{m}_{light} - \dot{m}_{dark}$), qi denotes the power density of solar simulator in the process of solar water evaporation experiment. Furthermore, h_{LV} denotes the sensible heat and enthalpy of the total liquid-vapor phase-change, which is calculated using equation:

$$h_{LV} = C\Delta T + \Delta h$$

Where C denotes the specific heat capacity of water (4.18 J g^{-1} K^{-1}), ΔT denotes the temperature increasement of water, and Δh denotes the enthalpy of vaporization on the relative temperature. As reported in a previous study, h_{LV} was approximately 2256.4 kJ kg^{-1}.

Comparing the efficiency of the evaporator made of two different molecules, between 2:00 p.m. and 5:00 p.m. on the same day, Under the environmental conditions of a temperature of 25 °C (±0.5 °C) and a relative humidity of 45% RH (±3% RH):

For IEIC-4F with hierarchical porous structure:

$$\dot{m}_{light} = 1.5608 \text{ kg m}^{-2} \text{ h}^{-1};\ \dot{m}_{dark} = 0.1810 \text{ kg m}^{-2} \text{ h}^{-1}$$

$$\dot{m} = \dot{m}_{light} - \dot{m}_{dark} = 1.5608 - 0.1810 = 1.3798 \text{ kg m}^{-2} \text{ h}^{-1}$$

$$h_{LV} \approx 2256.4 \text{ kJ kg}^{-1};\ q_i = 100 \text{ mW cm}^{-2}$$

$$\eta = (1.3798 \text{ kg m}^{-2} \text{ h}^{-1} \times 2256.4 \text{ kJ kg}^{-1}) / 100 \text{ mW cm}^{-2} = 86.4\%$$

For ITIC-4F with hierarchical porous structure:

$$\dot{m}_{light}= 1.2286 \text{ kg m}^{-2} \text{ h}^{-1};\ \dot{m}_{dark} = 0.1810 \text{ kg m}^{-2} \text{ h}^{-1}$$

$$\dot{m} = \dot{m}_{light} - \dot{m}_{dark}=1.2286 - 0.1810 =1.3798 \text{ kg m}^{-2} \text{ h}^{-1}$$

$$h_{LV} \approx 2256.4 \text{ kJ kg}^{1};\ q_i = 100 \text{ mW cm}^{-2}$$

$$\eta = (1.0476 \text{ kg m}^{-2} \text{ h}^{-1} \times 2256.4 \text{ kJ kg}^{-1}) /100 \text{ mW cm}^{-2} = 65.7\%$$

Comparing the efficiency of the evaporator made of two different sponge bases, between 2 and 5 p.m. on the same day, under the conditions of a temperature of 27 °C (±0.5 °C) and a relative humidity of 41% RH (±3% RH):

For IEIC-4F with hierarchical porous structure:

$$\dot{m}_{light}= 1.7600 \text{ kg m}^{-2} \text{ h}^{-1};\ \dot{m}_{dark} = 0.2952 \text{ kg m}^{-2} \text{ h}^{-1}$$

$$\dot{m} = \dot{m}_{light} - \dot{m}_{dark}=1.7600 - 0.2952 =1.4648 \text{ kg m}^{-2} \text{ h}^{-1}$$

$$h_{LV} \approx 2256.4 \text{ kJ kg}^{-1};\ q_i = 100 \text{ mW cm}^{-2}$$

$$\eta = (1.4648 \text{ kg m}^{-2} \text{ h}^{-1} \times 2256.4 \text{ kJ kg}^{-1}) /100 \text{ mW cm}^{-2} = 91.8\%$$

For IEIC-4F with only macroporous structure:

$$\dot{m}_{light}= 1.\ 4799 \text{ kg m}^{-2} \text{ h}^{-1};\ \dot{m}_{dark} = 0.2952 \text{ kg m}^{-2} \text{ h}^{-1}$$

$$\dot{m} = \dot{m}_{light} - \dot{m}_{dark}= 1.4799 - 0.2952 =1.1847 \text{ kg m}^{-2} \text{ h}^{-1}$$

$$h_{LV} \approx 2256.4 \text{ kJ kg}^{-1};\ q_i = 100 \text{ mW cm}^{-2}$$

$$\eta = (1.1847 \text{ kg m}^{-2} \text{ h}^{-1} \times 2256.4 \text{ kJ kg}^{-1}) /100 \text{ mW cm}^{-2} = 74.3\%$$

Antibacterial experiments

Experimental method:

Select an appropriate amount of mature colonies, place them in 5 mL of liquid medium and incubate at 37 ℃ for 6-8 hours until the OD600 reaches approximately 0.5. Adjust the pH to 7.4 with phosphate-buffered saline (PBS), then dilute the bacterial solution to a bacterial count of 10^6. Next, add 5 mL of the bacterial solution to the

sample for cultivation and expose the sample to xenon light. Cultivate at 37 ℃ for 24 hours, then take the bacterial solution from the culture liquid for counting to confirm the sterilization rate.

Source and cultivation of the algal samples

The algal solution used for the anti-algae test was an expanded algal solution purchased (~ 5×10^6 cells mg^{-1}) from commercial platform. The algal strain used was Microcystis aeruginosa. The algal solution was mixed with deionized water at a ratio of 1:3 to prepare a 250 mL algal culture solution, and 0.425 g of bg11 culture medium was added. The culture solution was transferred to a 250 mL conical flask and sealed with clean paper. The cultivation conditions were as follows: under an LED light of approximately 5000 lx, with 12 hours of light and 12 hours of darkness each day, and maintained at a temperature of 27 °C (±1.0 °C). The flasks were shaken 2 or 3 times daily in the morning and evening to ensure adequate dissolved air in the water and to ensure the healthy growth of the algae.

Forward cultivation method

To investigate the material's ability to inhibit algae through photocatalysis, the initial algae solution (with the same ratio as mentioned above) that had not been expanded was evenly divided into three groups and transferred to 100 mL beakers. Each beaker contained 50 mL of algae solution. In the experimental group, the control group, and the natural growth group, a sponge loaded with PM6: IEIC-4F and a blank sponge were respectively placed in the experimental group and the control group, and the evaporator was suspended freely in the upper layer of the water body. To highlight the material's photocatalytic function, under an LED light condition of approximately 5000

lx with continuous illumination, the cultivation conditions were controlled at 27 °C (±1 °C), and the shaking bottle habit was maintained. The algae growth and the absorbance in the ultraviolet-visible spectrum of the algae solution were observed after 7 days.

Reverse treatment experiment:

A reverse treatment experiment was performed in a sandwich-type beaker (Figure S19), which functioned as a photocatalytic anti-algae simulator. The device was constructed following Fan et al.'s method[14] for inorganic photocatalytic anti-algae materials. 50 mL of algal medium (diluted to 2.5×10^6 cells mL^{-1}, approximately) was added; the solar lamp simulator, equipped with UV400 and AM1.5 lenses, was adjusted to 1200 W m^{-2}. The experimental group used a hierarchical porous sponge loaded with PM6: IEIC-4F, while a blank sponge served as the control. Both groups underwent 6 h of photocatalytic treatment: at the 4th hour, 4 mL of medium was sampled for CLSM observation. After 6 h treatment, the medium was transferred to a clean beaker for secondary cultivation, with 0.085 g of BG11 medium added to supply algal nutrients. The experimental and control groups were simultaneously cultured under the aforementioned 5000 lx LED lights and 27 °C (±1 °C) conditions. On the 7th day, algal growth status and OD values were measured to evaluate algal regeneration ability post-photocatalysis.

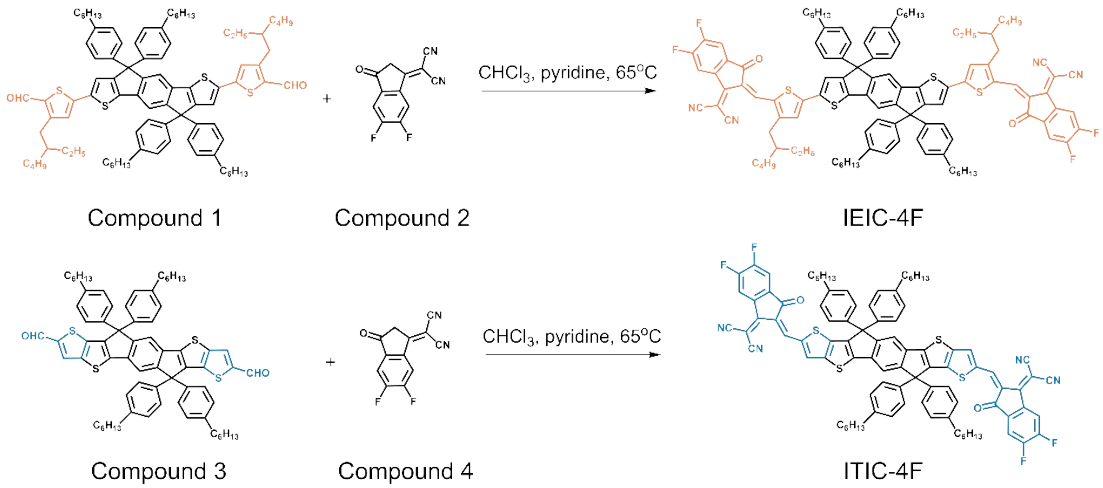

Scheme S1 Synthetic routes to IEIC-4F and ITIC-4F.

Scheme S2 The preparation procedure of evaporator with organic small molecules.

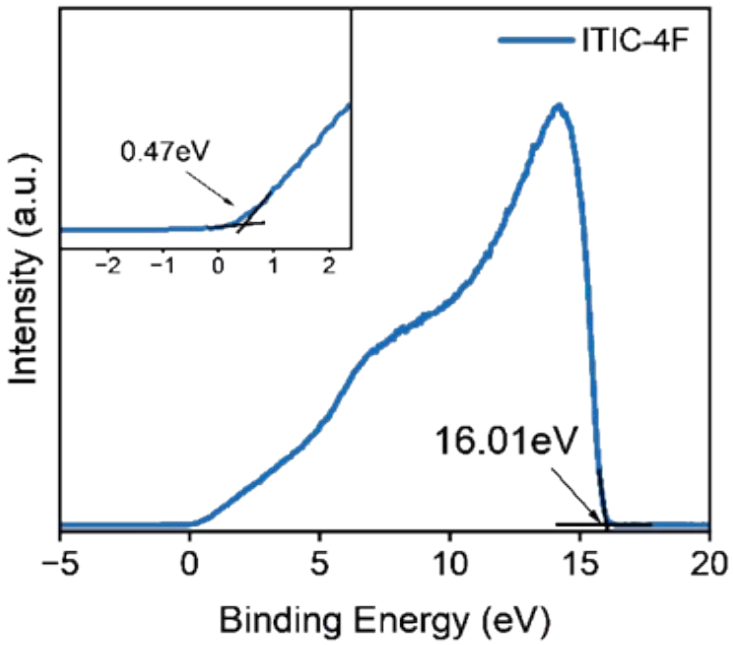

Figure S1 The UPS of ITIC-4F.

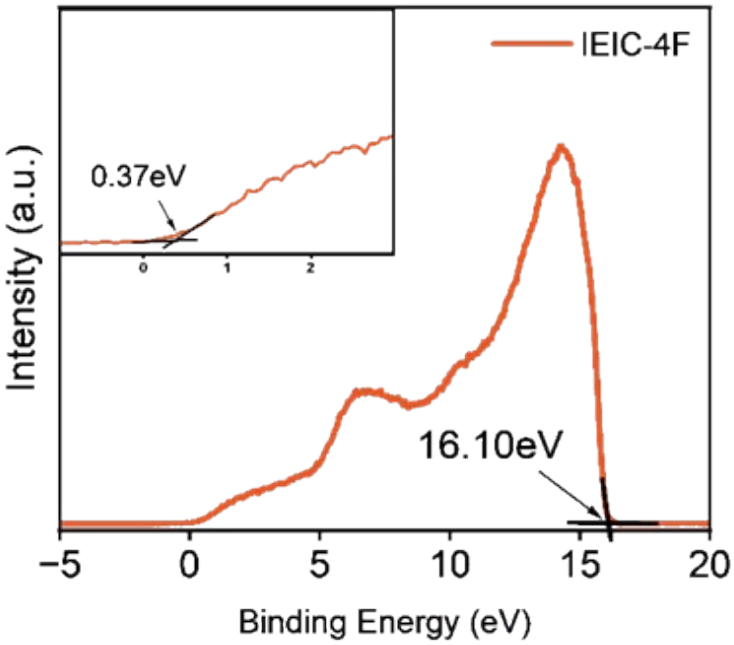

Figure S2 The UPS of IEIC-4F.

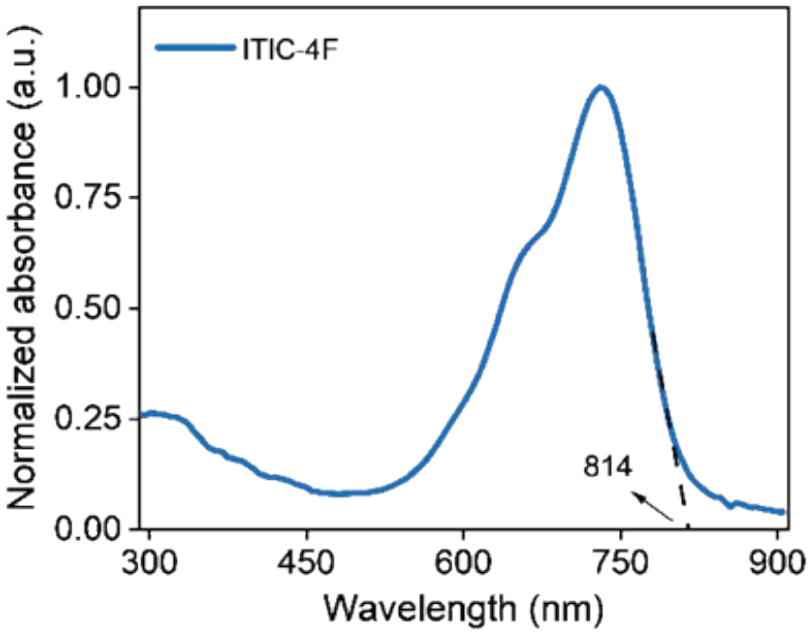

Figure S3 UV-Vis spectra of ITIC-4F in film.

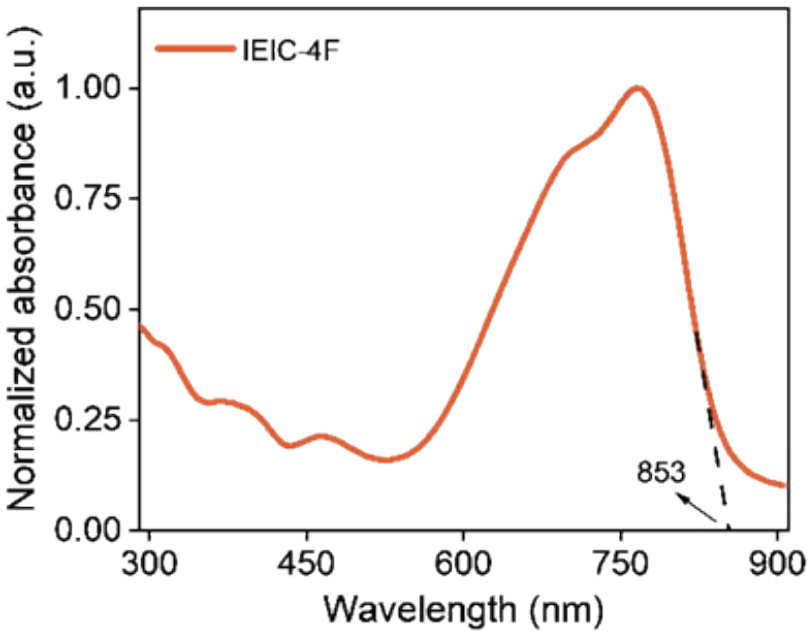

Figure S4 UV-Vis spectra of IEIC-4F in film.

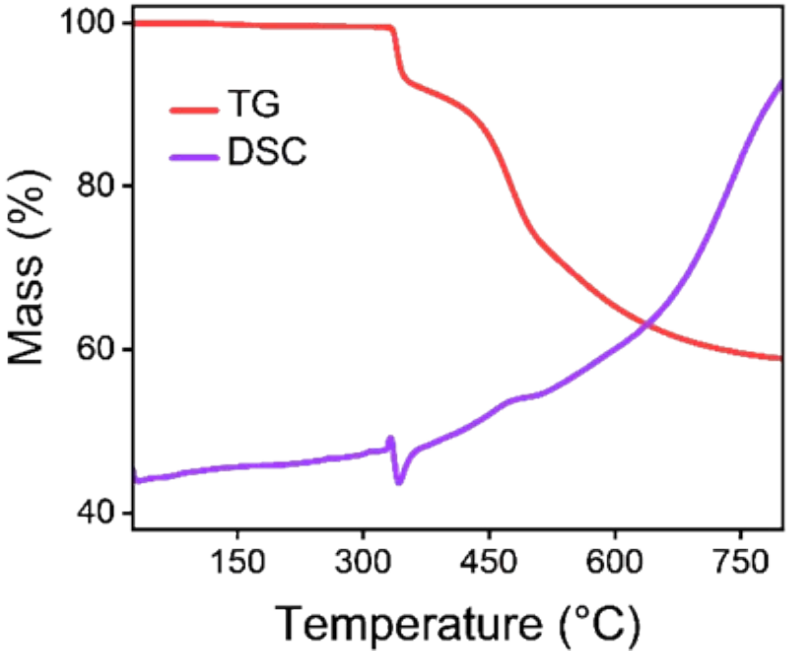

Figure S5 The TG-DSC of ITIC-4F.

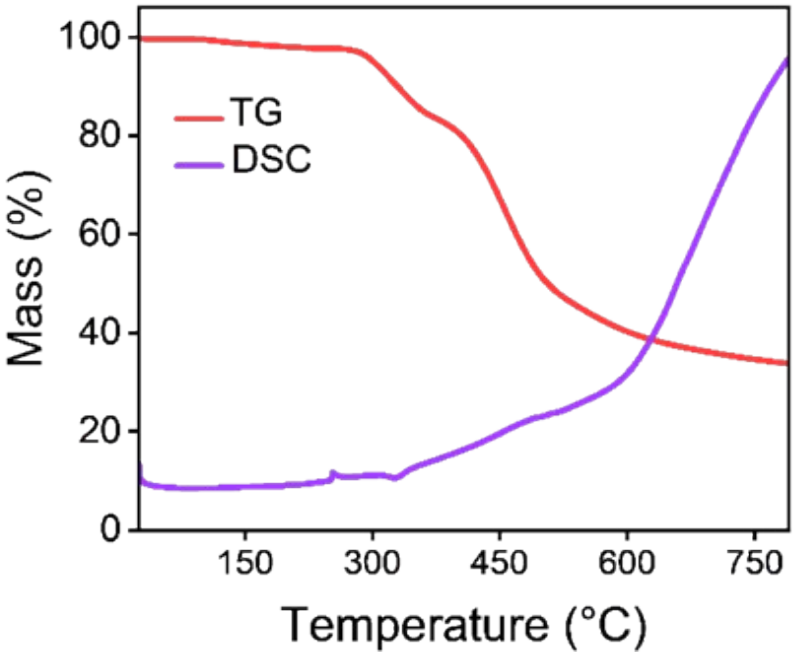

Figure S6 The TG-DSC of IEIC-4F.

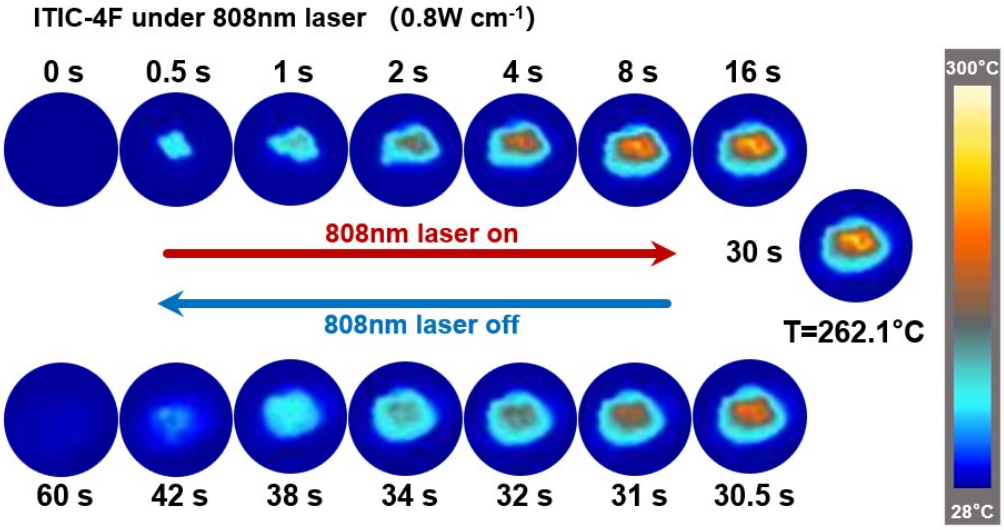

Figure S7 The infrared thermal photos of the ITIC-4F under laser irradiation.

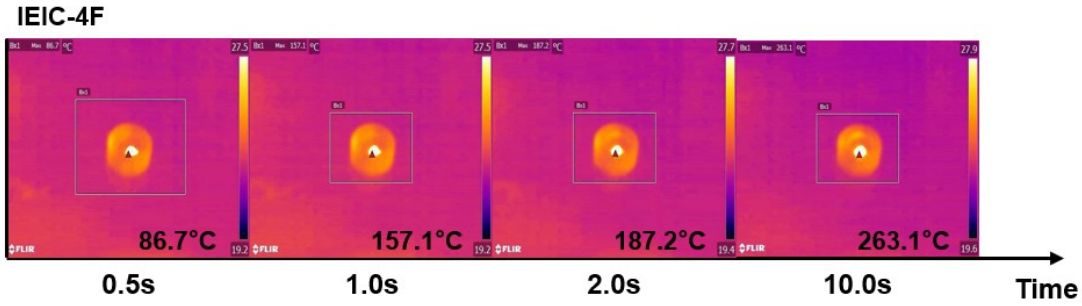

Figure S8 Infrared thermal imaging photos of the temperature rise of IEIC-4F under the irradiation of an 808 nm laser with a power density of 1.0 W cm^{-2}.

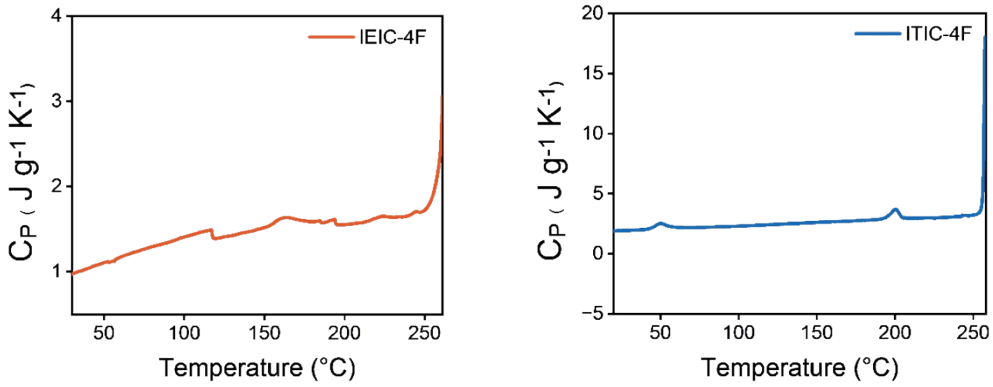

Figure S9 The average C_p of IEIC-4F and ITIC-4F.

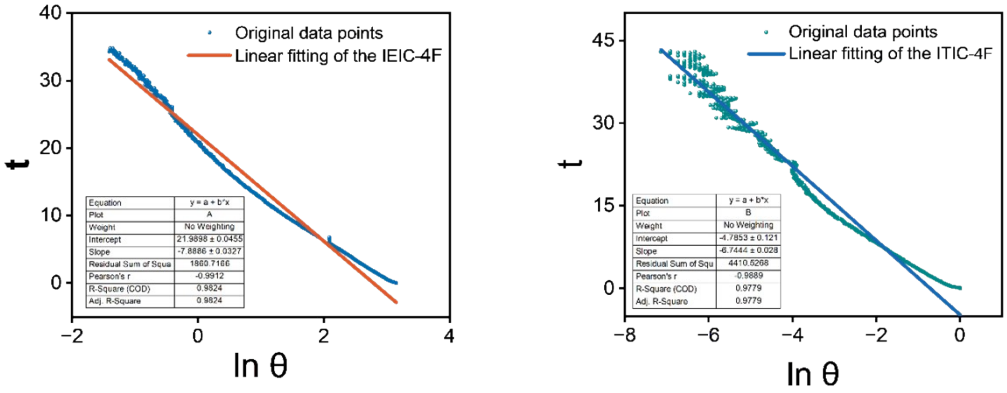

Figure S10 The calculation process of τ_S for IEIC-4F and ITIC-4F

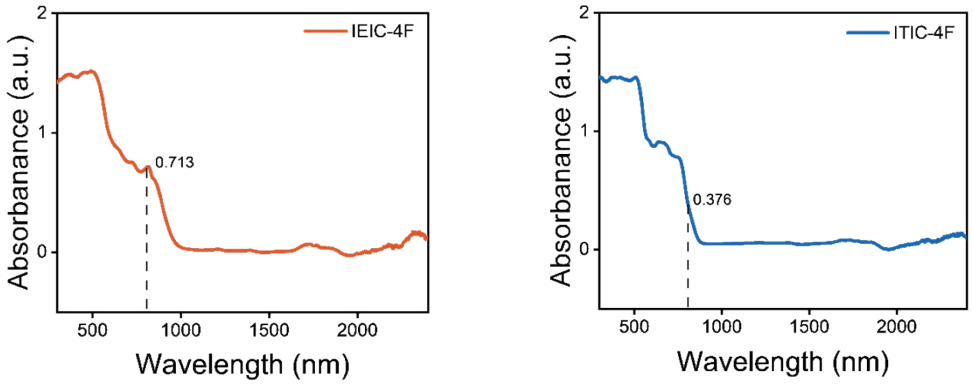

Figure S11 Absorption of IEIC-4F and ITIC-4F (calibrated with baritite).

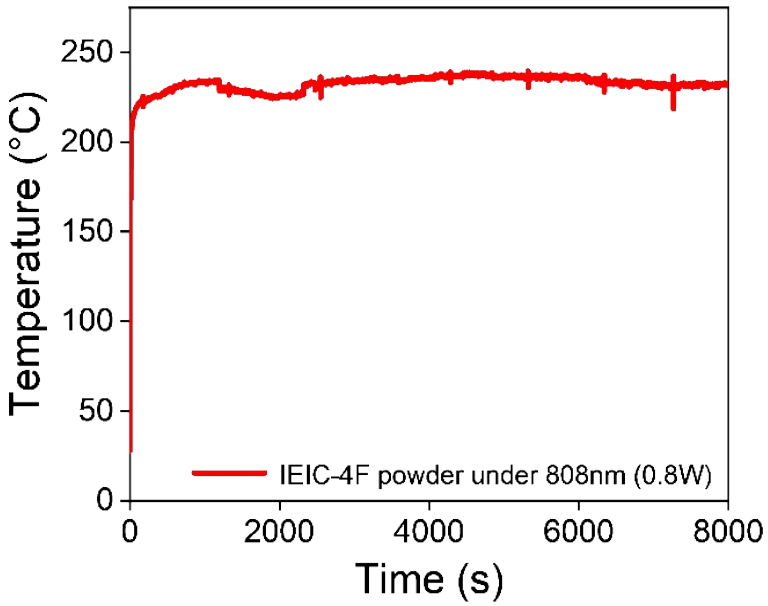

Figure S12 The 2-hour temperature profile of IEIC-4F under irradiation with an 808 nm laser (power density: 0.8 W cm^{-2}).

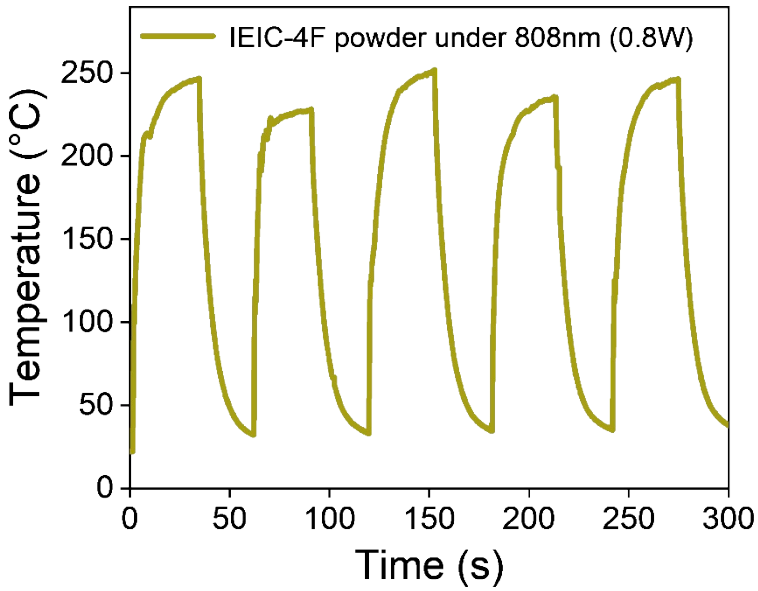

Figure S13 5 photothermal conversion cycles of IEIC-4F powder samples under 808 nm, 0.8 W cm^{-2} laser irradiation.

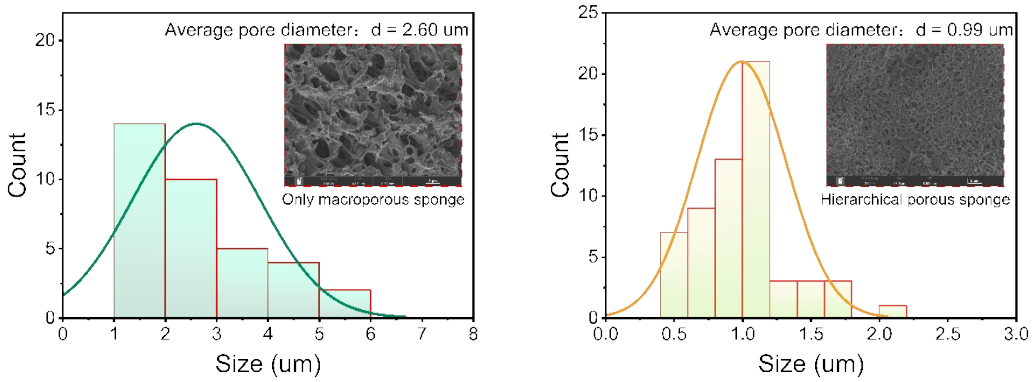

Figure S14 Pore size distribution of sponges with different micro-nano structures

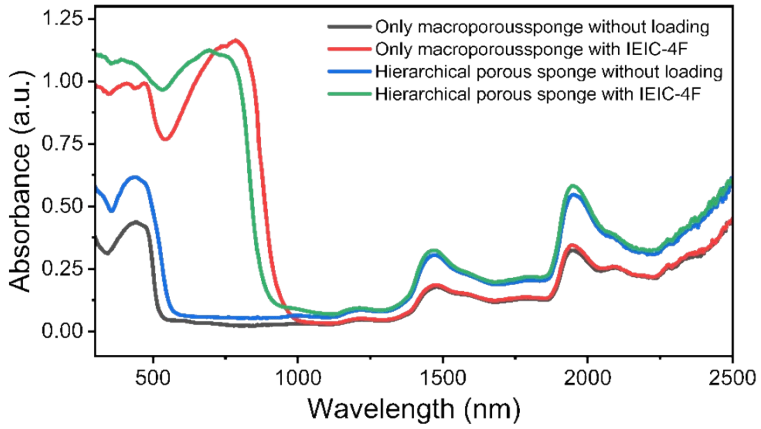

Figure S15 Diffuse reflection spectra of sponges with different micro-nano structures loaded with IEIC-4F and the unloaded control group.

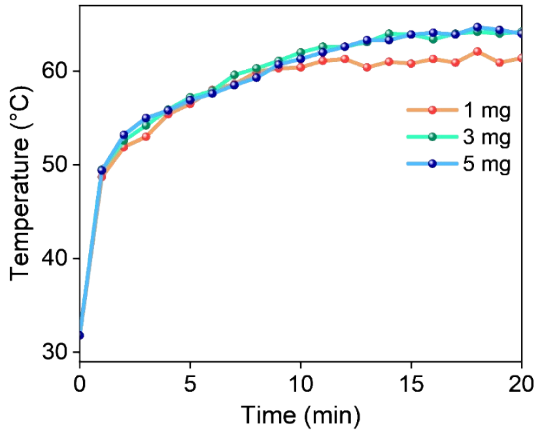

Figure S16 Variation of temperature with time in air for the IEIC-4F-evaporator with

loadings (1 mg, 3 mg and 5 mg) under simulated sunlight of 1000 W m^{-2} solar irradiation within 20 min.

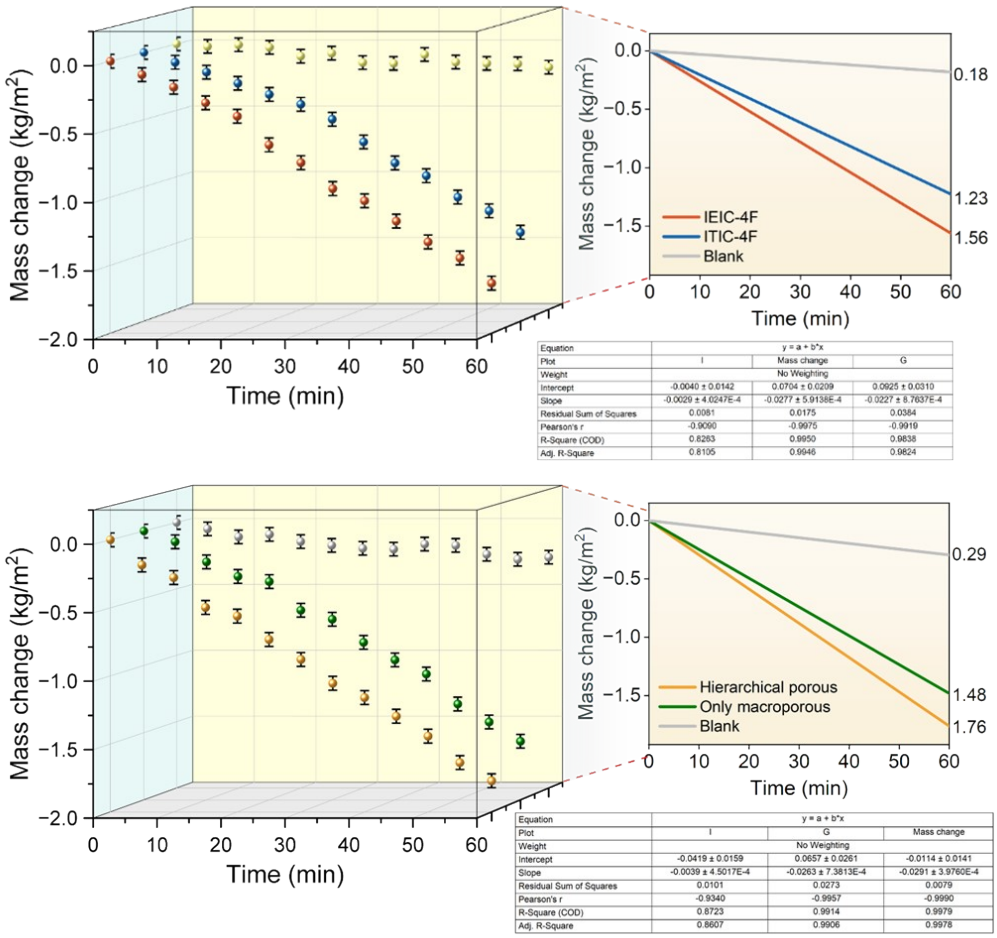

Equation	y = a + b*x		
Plot	I	Mass change	G
Weight	No Weighting		
Intercept	-0.0040 ± 0.0142	0.0704 ± 0.0209	0.0925 ± 0.0310
Slope	-0.0029 ± 4.0247E-4	-0.0277 ± 5.9158E-4	-0.0227 ± 8.7637E-4
Residual Sum of Squares	0.0081	0.0175	0.0384
Pearson's r	-0.9090	-0.9975	-0.9919
R-Square (COD)	0.8263	0.9950	0.9838
Adj. R-Square	0.8105	0.9946	0.9824

Equation	y = a + b*x		
Plot	I	G	Mass change
Weight	No Weighting		
Intercept	-0.0419 ± 0.0159	0.0657 ± 0.0261	-0.0114 ± 0.0141
Slope	-0.0039 ± 4.5017E-4	-0.0263 ± 7.3813E-4	-0.0291 ± 3.9760E-4
Residual Sum of Squares	0.0101	0.0273	0.0079
Pearson's r	-0.9340	-0.9957	-0.9990
R-Square (COD)	0.8723	0.9914	0.9979
Adj. R-Square	0.8607	0.9906	0.9978

Figure S17 The original data points of the simulated water evaporation experiment and the process of linear fitting.

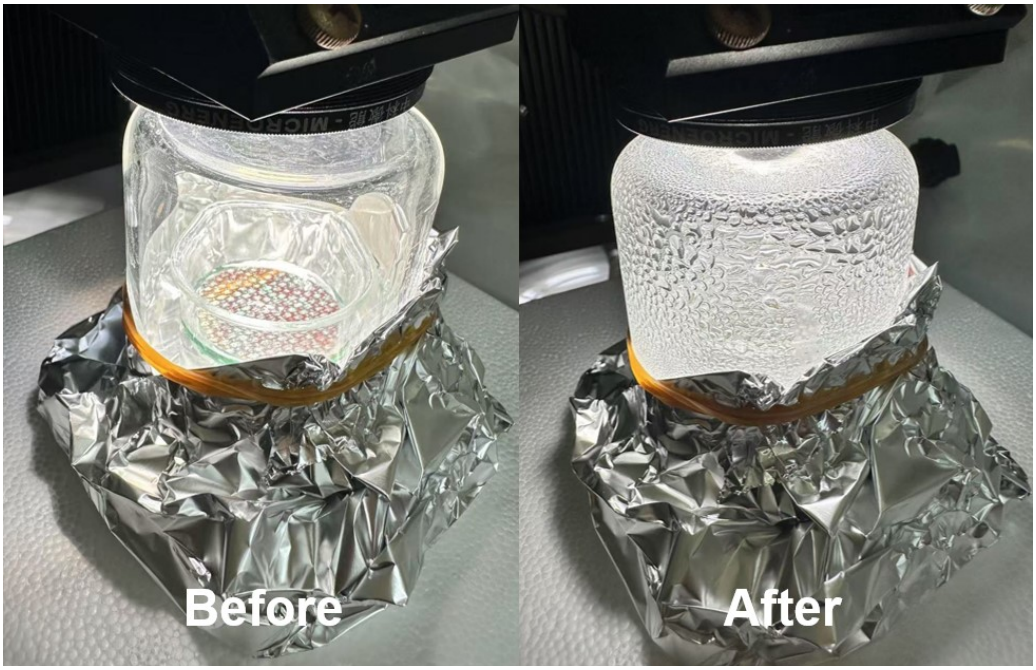

Figure S18 Digital images of the simple seawater desalination device.

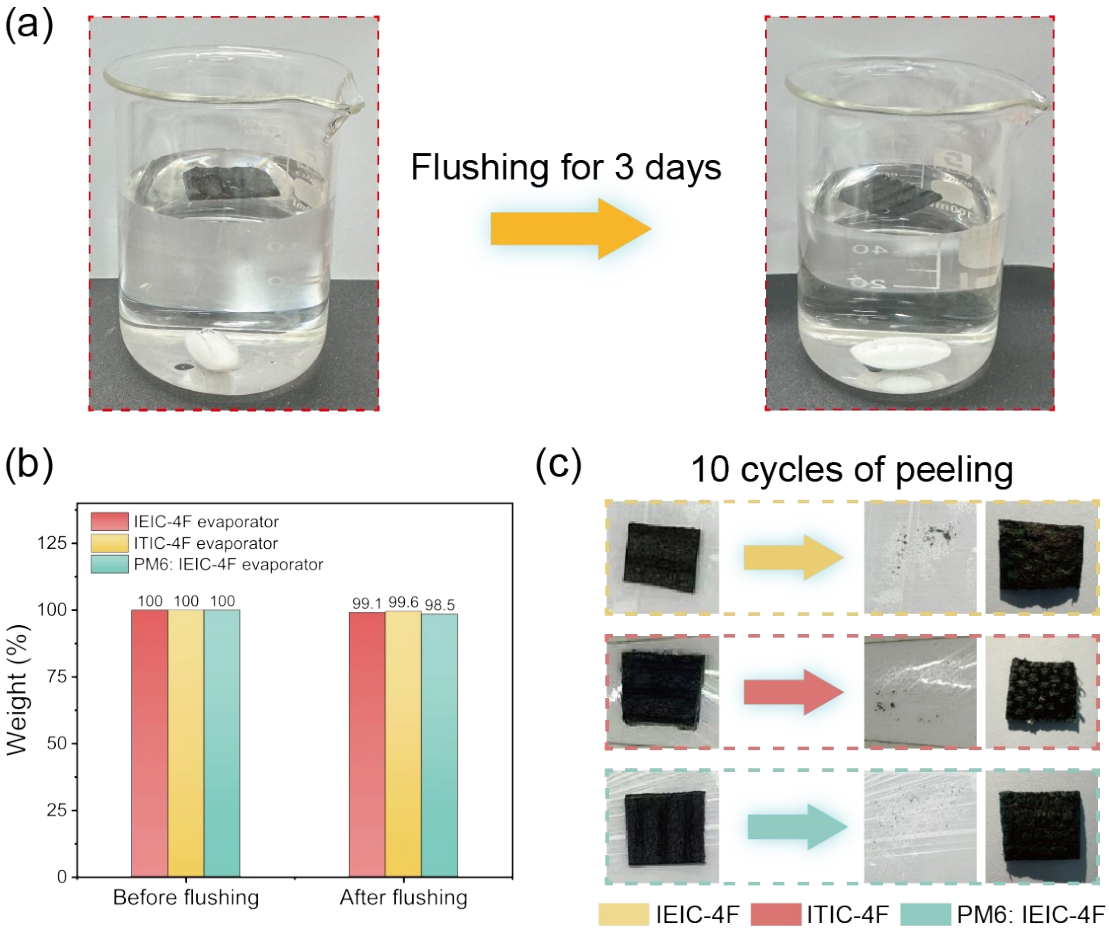

Figure S19 (a) Photographs of the mechanical stability tests of evaporator. (b)

Negligible mass changes of IEIC-4F/ITIC-4F/PM6: IEIC-4F evaporators before and after the flushing. (c) Photographs of the results of 10 cycles of peeling. (The black debris in the middle figure is wood sponge obtained via mechanical peeling, which appears black because it is loaded with photothermal materials)

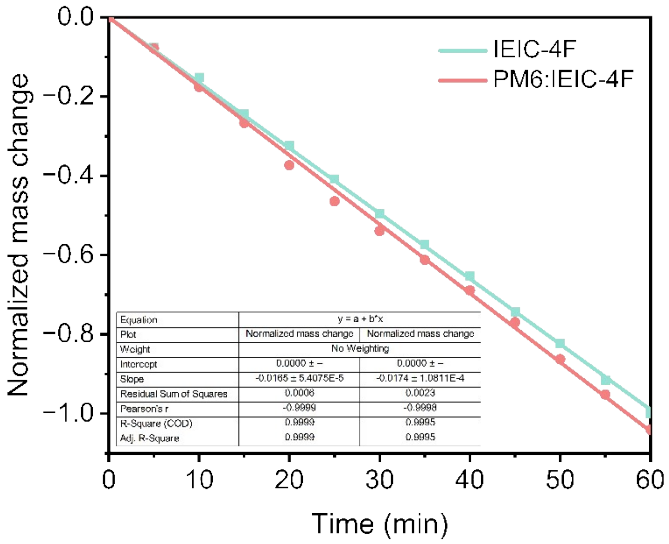

Figure S20 Water evaporation rates of IEIC-4F and PM6: IEIC-4F under 1 Sun irradiation

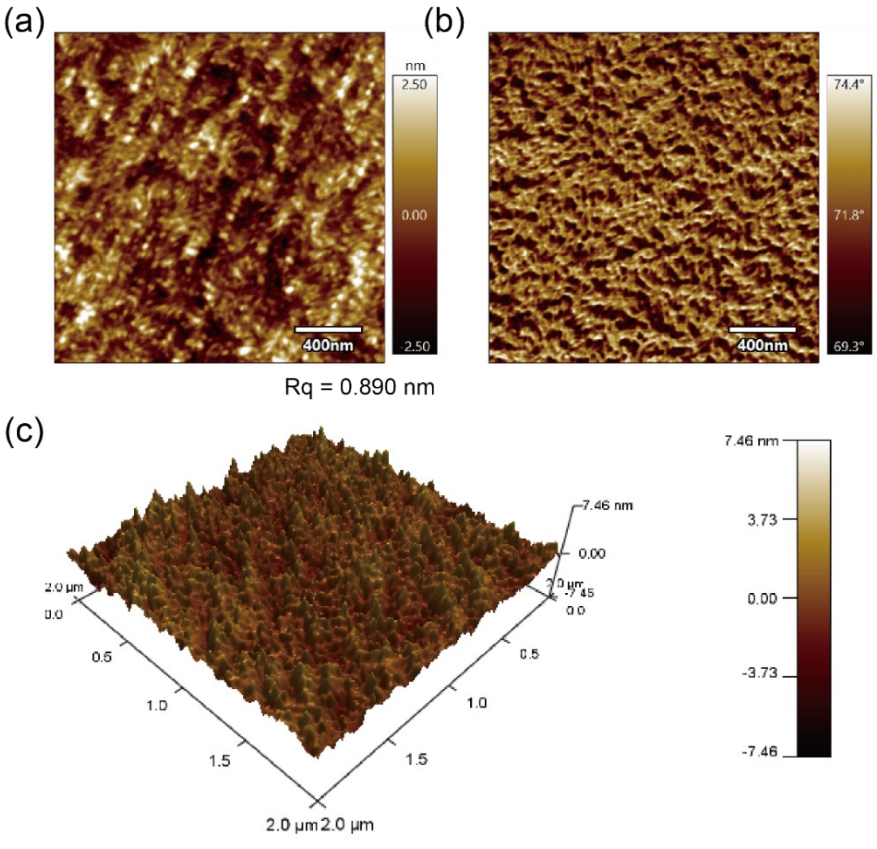

Figure S21 AFM images of PM6: IEIC-4F: (a) 2D height map. (b) phase image. (c) 3D height map.

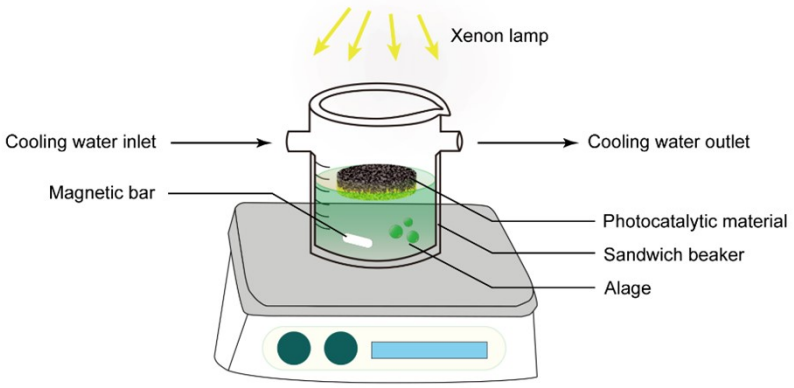

Figure S22 Schematic diagram of the organic photocatalytic anti-algae device.

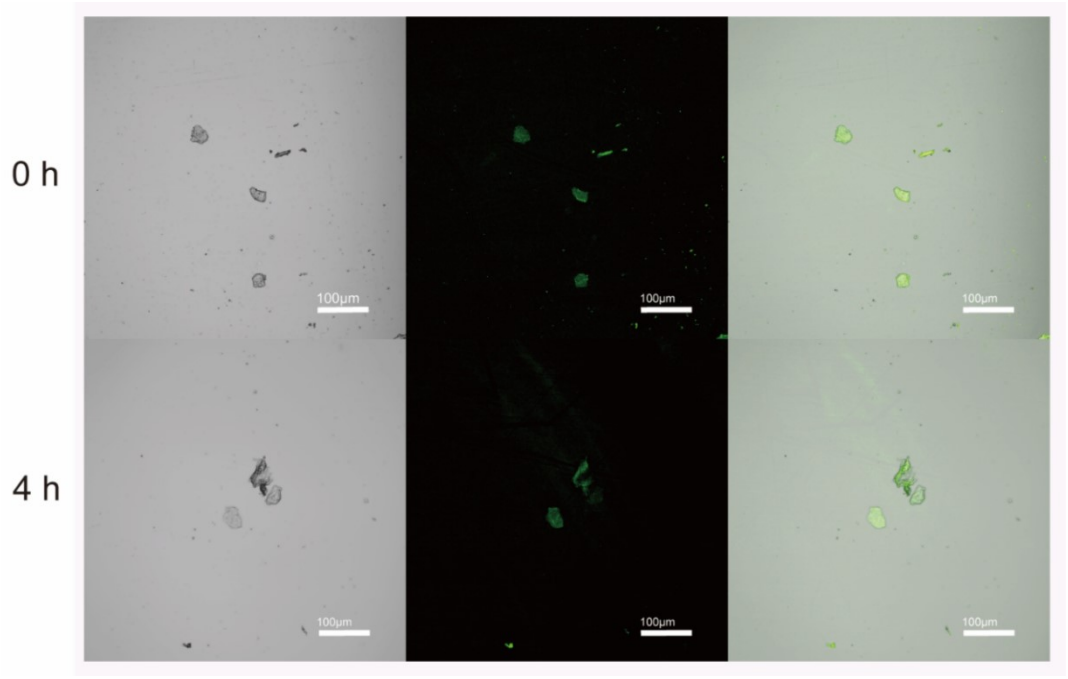

Figure S23 Confocal laser scanning microscopy (CLSM) images of algal cells at 0 h and 4 h photocatalytic treatment.

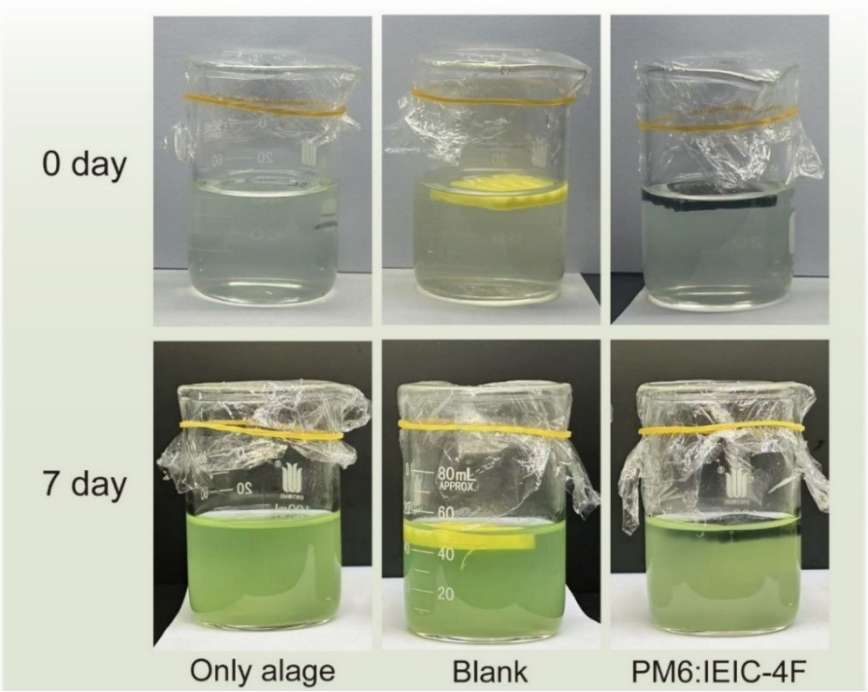

Figure S24 Images of cultured algae in natural growth group, control group, and experimental group at 0 day and 7 days of cultivation.

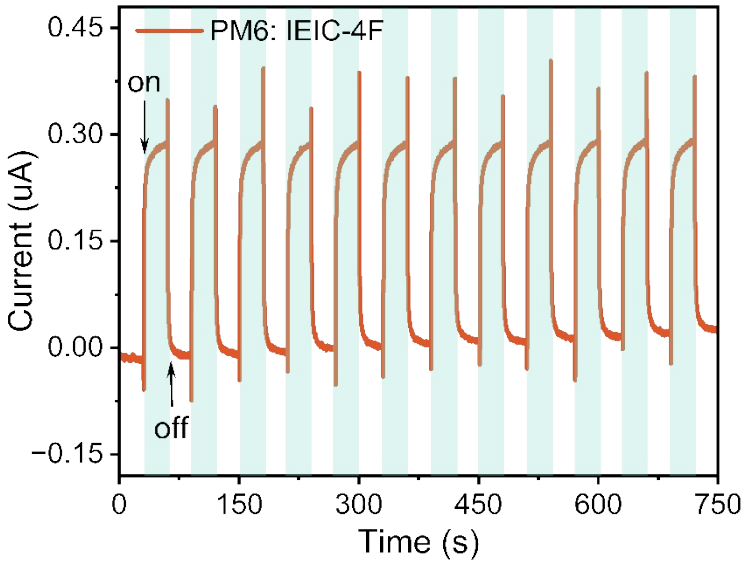

Figure S25 Photocurrent response of PM6: IEIC-4F under 10 light irradiation cycles.

Table S1 Antibacterial rate of materials after photocatalyst.

	IEIC-4F	IEIC-4F (with ROS scavenger)	ITIC-4F
antibacterial rate (*Escherichia coli*)	99.90%	33.5%	99.2%
antibacterial rate (*Staphylococcus aureus*)	99.90%	48.7%	99.5%

Notes and References

1 Y. Lin, Z.-G. Zhang, H. Bai, J. Wang, Y. Yao, Y. Li, D. Zhu, X. Zhan, *Energy Environ. Sci* 2015, **8**, 610.

2 T. J. Aldrich, M. Matta, W. Zhu, S. M. Swick, C. L. Stern, G. C. Schatz, A. Facchetti, F. S. Melkonyan, T. J. Marks, *J.Am.Chem.Soc* 2019, **141**, 3274.

3 M. Frisch, G. W. Trucks, H. B. Schlegel, G. E. Scuseria, M. A. Robb, J. R. Cheeseman, G. Scalmani, V. Barone, B. Mennucci, G. Petersson, Others, Gaussian 09, revision D. 01. In Gaussian, Inc., Wallingford CT: 2009.

4 S. Grimme, J. Antony, S. Ehrlich, H. Krieg, *J. Chem. Phys* 2010, **132**, 154104.

5 T. Clark, J. Chandrasekhar, G. W. Spitznagel, P. V. R. Schleyer, *J. Comput. Chem* 1983, **4**, 294.

6 T. Lu, F. Chen, *J. Chem. Phys* 2012, **33**, 580.

7 W. Humphrey, A. Dalke, K. Schulten, *J. Mol. Graph.* 1996, **14**, 33.

8 B. Hess, C. Kutzner, D. van der Spoel, E. Lindahl, *J. Chem. Theory Comp.* 2008, **4**, 435.

9 U. Essmann, L. Perera, M. L. Berkowitz, T. Darden, H. Lee, L. G. Pedersen, *J. Chem. Phys.* 1995, **103**, 8577.

10 B. Hess, H. Bekker, H. J. C. Berendsen, J. G. E. M. Fraaije, *J. Comput. Chem.* 1997, **18**, 1463.

11 Y. Cui, J. Liu, Z. Li, M. Ji, M. Zhao, M. Shen, X. Han, T. Jia, C. Li, Y. Wang, *Adv. Funct. Mater.* 2021, **31**, 2106247.

12 Z. Zhao, C. Chen, W. Wu, F. Wang, L. Du, X. Zhang, Y. Xiong, X. He, Y. Cai, R. T. K. Kwok, J. W. Y. Lam, X. Gao, P. Sun, D. L. Phillips, D. Ding, B. Z. Tang, *Nat. Commun.* 2019, **10**.

13 Z. Wei, W. Hong, H. Geng, C. Wang, Y. Liu, R. Li, W. Xu, Z. Shuai, W. Hu, Q.

Wang, *Adv. Mater.* 2010, **22**, 2458.

14 G. Fan, J. Zhang, J. Zhan, J. Luo, J. Lin, F. Qu, B. Du, D. Tang, B. Xie, Z. Yan, *J. Hazard. Mater.* 2021, **419**.